Boron-doped Ni/SBA-15 catalysts with enhanced coke resistance and catalytic performance for dry reforming of methane

Sharanjit Singh [a], Trinh Duy Nguyen [b], Tan Ji Siang [a], Pham T.T. Phuong [c], Nguyen Huu Huy Phuc [d], Quang Duc Truong [e], Su Shiung Lam [f], Dai-Viet N. Vo [a, g, *]

[a] Faculty of Chemical & Natural Resources Engineering, Universiti Malaysia Pahang, Lebuhraya Tun Razak, Gambang, 26300, Pahang, Malaysia
[b] NTT Hi-tech Institute, Nguyen Tat Thanh University, 300A Nguyen Tat Thanh Street, District 4, Ho Chi Minh City, 755414, Viet Nam
[c] Institute of Chemical Technology, Vietnam Academy of Science and Technology, 1 Mac Dinh Chi Str., Dist.1, Ho Chi Minh City, Viet Nam
[d] Department of Electrical and Electronic Information Engineering, Toyohashi University of Technology, 1-1 Hibarigaoka, Tempaku, Toyohashi, Aichi, 441-8580, Japan
[e] Institute of Multidisciplinary Research for Advanced Materials, Tohoku University, Katahira 2-1-1, Aoba-Ku, Sendai, 980-8577, Japan
[f] Pyrolysis Technology Research Group, Eastern Corridor Renewable Energy Group, School of Ocean Engineering, Universiti Malaysia Terengganu, 21030, Kuala Nerus, Terengganu, Malaysia
[g] Center of Excellence for Green Energy and Environmental Nanomaterials (CE@GrEEN), Nguyen Tat Thanh University, 300A Nguyen Tat Thanh, District 4, Ho Chi Minh City, 755414, Viet Nam

ARTICLE INFO

ABSTRACT

Nickel-based heterogeneous catalysts have shown promising results in many industrial-scale catalytic reforming processes and hydrocarbon reforming reactions such as dry reforming of methane (DRM). However, it is also reported that Ni-based catalysts generally show less resistance to the carbonaceous deposition, which ultimately causes their rapid deactivation during the reaction. One possible solution to improve the coke resistance is the addition of a promoter to the catalyst, which has shown successful results to reduce the coke formation. Therefore, this study also aimed to prepare boron-promoted Ni-based catalysts and investigate their efficiency for DRM reactions. A series of different catalysts with 10% nickel and x% boron (x: 1%, 2%, 3%, and 5%) were prepared by using an ordered mesoporous silica as a support and tested in DRM. The results demonstrated that boron-promoted Ni/SBA-15 catalysts obtained significant catalytic activity for CH_4 and CO_2 conversions. Meanwhile, it was noticed that a lower concentration of boron (1 and 2%) was more favourable to achieve higher catalytic activity, whereas the higher concentration (3% and 5%) resulted in a comparatively lower conversion for CH_4 and CO_2. Evidently, the higher activity of 2% B-promoted catalyst was ascribed to the synergistic effect of high surface area and lower crystallite size that greatly improved the active sites accessibility. Moreover, the results confirmed 14% carbon deposition on unpromoted (NS) catalyst and it was reduced to 1.3% for 2% boron-promoted catalyst owing to the presence of B-OH species on catalyst surface.

© 2019 Energy Institute. Published by Elsevier Ltd. All rights reserved.

1. Introduction

Synthetic gas (syngas) is a versatile building block to produce synthetic fuels (such as dimethyl ether, methanol, and long-chain hydrocarbons) in petrochemical industries [1,2]. The dry reforming of methane (DRM) reaction has been substantially examined to convert methane and carbon dioxide gases to useful syngas [3]. However, DRM reaction requires a highly active catalyst to promote the conversion of these gases to achieve high conversion and stability. Different types of heterogenous catalysts have been investigated in DRM reaction but noble-metal catalysts have shown the most promising results so far. However, due to their low availability and high cost, the cost-efficient nickel-based catalyst is the most preferable choice since it exhibits comparable performance for reforming reactions [4,5]. The imminent

---

catalyst deactivation from carbon formation in nickel-based catalyst is a major concern. Therefore, the preparation of active catalyst with high resistance to carbon is still a hot topic in DRM.

The formation of surface carbon is generally considered as a key intermediate step in methane reforming reaction. In the presence of low oxygen species at the surface, this surface carbon can diffuse into the subsurface of octahedral sites to entice carbon build-up or interact with outer carbon to form graphene islands. Therefore, several basic or alkaline metals and rare earth oxides such as CeO_2 [6,7], La_2O_3 [8], ZrO_2 [9], MgO [10], and CaO [11] have been employed to improve surface oxygen atoms, which can react with carbon species and convert to CO, thus impede the carbon deposition. Many efforts have been made to control the carbon deposition over nickel-based catalysts. In this regard, the strategy of promotion of different nickel-based catalysts is turned out to be an efficient technique to enable high resistance to carbon deposition and perform high activity as well as stability (see Table 1).

Recently, boron has gained significant research interests for the role of promoter due to its excellent tendency to mitigate coke nucleation sites. Saeys et al. studied the effect of boron on Co surface with density functional theory (DFT) calculations and proved that boron mimics the adsorption of carbon by occupying the octahedral sites of the first subsurface layer on metal and thus selectively blocking the diffusion of carbon into its lattice, hence lowers the carbon formation [12]. In past decades, effect of boron on Al_2O_3-supported nickel catalysts has been investigated. For example, 1% boron promoted on 15%Ni-alumina catalyst decreased the carbon deposition by 80% in steam reforming of methane [13]. In another study, the nickel-based catalyst promoted with boron was employed for the Fischer-Tropsch reaction. The results found that the addition of boron reduced the rate of deactivation by six-folds without affecting the catalytic performance [14]. More recently, it has been demonstrated that the addition of boron to Ni/Al_2O_3 catalyst not only reduced the carbon deposition but also controlled the size of Ni particles [15].

It is evident from the earlier studies that boron promoter could be utilized for hindering the carbon formation on the catalyst surface. However, no previous study has explored the combined effects of boron and high surface area of mesoporous SBA-15 support for dry reforming of methane; therefore, a comprehensive investigation is required to shed more light on the role of boron promotion. The comparative examination of catalytic performance for different boron loadings on SBA-15 supported nickel catalysts was the main aim of this study. Verifying the function of boron promoter on simultaneously controlling carbon formation and size of nickel particles was another objective of this investigation. Thus, a series of different weight percentages of boron (1%, 2%, 3%, and 5%) loaded on SBA-15 supported nickel catalysts were synthesized and tested for DRM.

2. Experimental

2.1. Catalyst preparation

A conventional and facile hydrothermal technique was employed to synthesize mesoporous SBA-15 support. In brief, 5.8 g of non-ionic triblock poly (ethylene glycol)-block-poly (propylene glycol)-block-poly (ethylene glycol) surfactant (commercially abbreviated as PEG-PPG-PEG or Pluronic® P-123, supplied by Sigma-Aldrich Chemicals, St. Louis, Missouri, US) was dissolved in HCl (1.6 M, 200 ml, Merck Millipore, Burlington, Massachusetts, US) solution to maintain a pH = 1. Thereafter, the solution was stirred for 2 h on a magnetic hot plate at 313 K to properly dissolve the former surfactant template. Then, 12.9 g of tetraethyl orthosilicate, TEOS (Merck Millipore, Burlington, Massachusetts, US) was added dropwise into the solution and kept for stirring overnight. The hydrothermal aging was conducted in an autoclave (Teflon-lined stainless-steel vessel) for 24 h at 373 K under static conditions. The white precipitates were extracted by the paper filter and washed with deionized (D.I.) and distilled water before being dried for 12 h at 333 K. Afterward, the obtained solid powder was transferred to a furnace (Bemaford, Sheffield, UK) for eliminating structure-directing surfactant by air-calcination at 823 K for 5 h to form the siliceous support with mesoporous structure.

The sequential incipient-wetness impregnation (SIWI) procedure was implemented for preparing the boron-promoted samples. In incipient-wetness impregnation (IWI) approach, freshly calcined mesoporous silica support was thoroughly mixed with a required amount of nickel nitrate solution (supplied by Sigma-Aldrich Chemicals, St. Louis, Missouri, US) using a vacuum rotary evaporator (BÜCHI Rotavapor R-200, Flawil, Switzerland) at temperature of 333 K for 2 h. After overnight drying at 333 K, the dried powder was air calcined at 1023 K for 5 h (2 K min^{-1}) to yield the 10 wt% Ni/SBA-15 catalyst. To prepare a series of boron-promoted catalysts, the required amount of boric acid (H_3BO_3, Sigma-Aldrich Chemicals, St. Louis, Missouri, US) was impregnated with the earlier prepared SBA-15 supported nickel catalyst using

Table 1
Summary of different promoters on Ni-based catalysts.

Catalyst type	Amount of nickel	Promoter type	Crystallite size of nickel (nm)/dispersion (%)	Reaction temperature (K)/[b]GHSV (mL g^{-1} h^{-1})	[c]Catalytic activity (X_1/X_2)	Catalyst deactivation/ Time-on-stream	References
Hexagonal-Boron Nitride-Ni/SBA-15	6.2%Nickel	[a]n.d.% Hexagonal Boron nitride	n.d./9.74%	1023/15000	90.5/100	0.2%/100 h	[16]
Boron-Ni/Al$_2$O$_3$	5%Nickel	5%Boron	7.1/n.d.	973/30000	75/67	13%/65 h	[17]
Boron-Ni/Al$_2$O$_3$	10%Nickel	5.6%Boron	5.1 ± 0.4/n.d.	973/30000	62.5/54	n.d./24 h	[15]
Y$_2$O$_3$-Ni/SBA-15	10%Nickel	3%Yttrium	10.5/9.2	973/36000	70.8/74.4	n.d./60 h	[18]
Sm$_2$O$_3$-Ni/SBA-15	10%Nickel	3%Samarium	9.7/10.0		70.6/74.4		
ZrO$_2$/Ni/SBA-15	10%Nickel	3%Zirconia	11.7/8.3		39.7/48.8		
Sm-Ni/SBA-15	10%Nickel	3%Samarium	7.3/13.8	1023/75000	69.6/73.6	n.d./25 h	[19]
Mg/Ni/SiO$_2$	8.4%Nickel	4.5%Magnesium	13/n.d.	1073/36000	78.5/80.6	n.d./30 h	[20]
Ce$_{0.75}$Zr$_{0.25}$O$_2$-10%Ni/SBA-15	10%Nickel	Ceria and Zirconia (Ce/Zr of 1.5)	9/n.d.	873/20000	42/48	39%/23 h	[21]
La$_2$O$_3$-10%Ni/SBA-15	5%Nickel	2%La$_2$O$_3$	3.1/n.d.	973/72000	83/86.5	n.d./10 h	[22]

[a] n.d.: Not defined.
[b] GHSV: Gas hourly space velocity.
[c] X_1 is CH$_4$ conversion and X_2 is CO$_2$ conversion.

the similar aforementioned method. These promoted catalysts were labelled as x%B-NS (with x: 1, 2, 3 or 5%), whereas the unpromoted catalyst was denoted as NS.

2.2. Catalytic characterization procedure

For analysing the crystal structure of both original and used catalysts, X-ray diffraction (XRD) analysis was performed using Rigaku Miniflex II (Akishima-shi, Tokyo, Japan) instrument which employs a Cu monochromatic anode as a source of X-rays of wavelength, $\lambda = 1.5418$ Å and was conducted at 15 mA and 30 kV. XRD patterns were examined within $3°-80°$ of 2θ range with a low scan rate of $1°$ per min and stride size of $0.02°$. Scherrer equation was used to measure crystallite size ($d_{crystal}$) was measured (Eq. (1)) [16,23].

$$d_{crystal}(nm) = \frac{0.94\lambda}{B \times \cos\theta} \tag{1}$$

The BET (Brunauer, Emmett and Teller) surface area was calculated by gas adsorption studies at temperature of 77 K on a volumetric adsorption analyzer (Micromeritics ASAP-2010, Norcross, Georgia). Barrett-Joyner-Hallender (BJH) method using desorption branch data was employed for measuring total pore volume and total pore size distribution. The morphology and element content in the 2%B-NS catalyst were determined by using the scanning electron microscope (SEM) coupled with energy-dispersive X-ray (EDX) spectroscopy analysis on Hitachi Tabletop Microscope TM3030Plus (Dillenburgstraat, Eindhoven, The Netherlands). H_2-temperature programmed reduction (H_2-TPR) profiles were obtained by using AutoChem II-2920 system (Norcross, Georgia, US) for analysing metal-support interaction, specimens were pre-heated in He gas for 30 min at 373 K with a flow rate of 50 ml min^{-1} to remove the volatile compounds. Pre-treated samples were then reduced with 10%H_2/Ar mixture in the temperature range of $373-1173$ K at flowrate of 50 ml min^{-1} and heating ramping of 10 K min^{-1}.

ATR-FTIR (Attenuated Total Reflectance - Fourier Transform Infrared) spectroscopy was scanned between 400 and 4000 cm^{-1} in Thermo Fisher Scientific Nicolet iS5 FTIR (Waltham, Massachusetts, US) spectrometer (equipped with iD7 ATR accessory) and the resolution of 4 cm^{-1} for each spectrum was used for studying the surface functionality of catalysts. All obtained spectra were interpreted by the OMNIC™ software version 8.0. Raman analyses were obtained to examine the deposition of carbonaceous species on spent catalysts. The study was performed within $100-2000$ cm^{-1} region in a JASCO NRS-3100 Raman spectrometer (Waltham, Massachusetts) employing 532 nm laser excitation. X-ray photoelectron spectroscopy (XPS) analysis was performed in the ULVAC-PHI 5000 VersaProbe II system (ΦULVAC-PHI, Inc., Chigasaki, Japan). A monochromatic Al Kα (hν = 1486.6 eV) X-ray radiation was employed as excitation source. Prior to data fitting, the binding energies of all spectra were referenced to the standard calibrated value of the adventitious carbon C 1s peak at 286.4 eV. The temperature-programmed oxidation (TPO) was employed to quantitatively calculate the amount of carbon formation on spent catalysts. It was conducted on a TA Instruments Q500 TGA (New Castle, Delaware, US). Spent catalyst (*ca.* 0.05 g) was initially heated for 30 min at 373 K in inert gas and then the temperature was increased linearly with 10 K min^{-1} from 373 K to 1023 K in purging 20%O_2/N_2 oxidizing mixture. High resolution transmission electron microscopy (HRTEM) images were captured via TOPCON EM-002B microscope (Naka-cho, Musashino-shi, Tokyo, Japan) operating at 200 kV. The specimens were homogeneously dispersed in ethanol using ultrasonic treatment and then placed onto Cu microgrid supported by a holey carbon film, prior to each analysis.

2.3. Dry reforming of methane reaction evaluation

The dry reforming of methane (DRM) reactions were performed in a tubular fixed-bed reactor with a stoichiometric feed ratio: $Q_{CH_4} : Q_{CO_2} = 1 : 1$ (Q_i: molar flow rate for reactant species i, mol s^{-1}) under ambient pressure at 1023 K. Sieved catalyst powder (about 0.1 g with an average particle size of $100-140$ μm) was positioned in the middle of the reactor (outer diameter = 9.5 mm, inner diameter = 7 mm and length = 40 cm) and placed vertical in the split temperature-controlled furnace. In order to activate the catalyst, 50%H_2/N_2 mixture at flowrate of 60 ml min^{-1} was purged through the catalyst bed at 1023 K for 2 h before each catalytic test. The total inlet flow rate of the reactants (CH_4 and CO_2) and N_2 diluent gas (maintained by calibrated Alicat Mass Flow controllers, Tucson, Arizona, US) with a gas hourly space velocity (GHSV) of 36 L g_{cat}^{-1} h^{-1} and flow rate of 60 ml min^{-1} were used to ensure insignificant heat transfer and mass transfer resistances for achieving intrinsic catalytic activity. Water, the by-product produced during the DRM reaction was condensed by a cold trap, whereas the residual water was further captured by drierite adsorption bed. The produced gases were examined in a Gas chromatograph (GC) equipped with Agilent 6890 Series GC system (Santa Clara, California, US). Prior to experiments, all mass flow controllers were calibrated using multiple-point calibration to assure the accuracy of experimental data and reproducibility. On the other hand, the GC data was further verified using N_2 internal standard, which was continuously co-fed with the reactants during reaction. Thus, conducted material balance found the minimal error within 0.59%–2.76% whereas the relative error among repeated runs at the same conditions was below 3.26%.

Reactant conversions, X_i (with i being CH_4 or CO_2) are calculated by Eq. (2).

$$X_i(\%) = \frac{Q_i^{In} - Q_i^{Out}}{Q_i^{In}} \times 100\% \tag{2}$$

whilst H_2/CO ratio, gaseous product yield, Y_j (j: H_2 or CO), and product selectivity, S_j were estimated from Eqs. (3)–(6), respectively.

$$H_2/CO\ ratio = \frac{Q_{H_2}^{out}}{Q_{CO}^{out}} \tag{3}$$

$$Y_{H_2}(\%) = \frac{Q_{H_2}^{Out}}{2Q_{CH_4}^{In}} \times 100\% \tag{4}$$

$$Y_{CO}(\%) = \frac{Q_{CO}^{Out}}{Q_{CH_4}^{In} + Q_{CO_2}^{In}} \times 100\% \tag{5}$$

and

$$S_j(\%) = \frac{Q_j^{Out}}{Q_{H_2}^{Out} + Q_{CO}^{Out}} \times 100\% \tag{6}$$

where Q^{In} and Q^{Out} (mol s^{-1}) signify the inlet molar flow rate and outlet molar flow rate in this order.

3. Results and discussion

3.1. Textural and morphological properties

Table 2 summarizes the textural characteristics of support, NS and x%B-NS catalysts. The N$_2$ adsorption/desorption isotherms are shown in Fig. 1. The results demonstrated that bare SBA-15 support, NS and x%B-NS (x: 1%–3%) showed a typical Langmuir type IV isotherm with H1 hysteresis loop, which represent highly ordered mesoporous structures with narrow pore size distribution of the cylindrical channels [24]. In addition, the capillary condensation of N$_2$ at a high relative pressure between P/P$_0$ = 0.53–0.83 indicates the uniform distribution of pores in the catalysts [25]. The SBA-15 support exhibited the largest BET surface area of 669.8 m^2 g^{-1} and 1.2 cm^3 g^{-1} of pore volume. A decrease in the BET surface area (538.7 m^2 g^{-1}) and total pore volume (0.9 cm^3 g^{-1}) was observed for unpromoted catalyst. This result reflected that some of the NiO particles were successfully inhabited by the support.

Furthermore, it was noticed that the concentration of boron from 1 to 3% in the catalysts did not affect the shape of isotherms as well as H1 hysteresis loop. However, the highest content of boron (5%) induced strong shrinkage or collapse of type IV isotherm and H1 hysteresis loop, which confirmed a slight decrease in the pore size. Evidently, the pore size in 3% boron promoted catalyst was 6.6 nm while the catalyst with 5% boron obtained a pore size of 4.1 nm. This decrease in pore size can be attributed to the higher acidity of catalyst due to a high concentration of boric acid (H$_3$BO$_3$) in the SBA-15 support. Thus, it can be suggested that thin pore walls of mesoporous support could be damaged during the catalyst preparation process that resulted in poor textural properties of the catalyst. Moreover, the higher concentration of H$_3$BO$_3$ precursor significantly reduced the average BET surface area and total pore volume of 5%B-promoted catalyst to 4.1 m^2 g^{-1} and 0.3 cm^3 g^{-1}, respectively as summarized in Table 2. This drastic decrease in BET surface area may be attributed to the pore blockage caused by B$_2$O$_3$ species entering into the micropore channels of SBA-15 support and agglomerating on support surface [26]. These findings are consistent with other studies which also observed a remarkable decrease in the BET surface area of B-promoted Ni/Al$_2$O$_3$, owing to high acidity rendered by H$_3$BO$_3$ at a high boron content of 12.3% [15]. The morphology and elemental composition of the selected 2%B-NS catalyst were further observed by using SEM-EDX analysis. The EDX analysis, SEM micrograph and corresponding elemental mapping are given in Fig. S1of supplementary data. The SEM micrograph shows that 2%B-NS catalyst displays the cotton-like surface morphology. In addition, the amount of nickel metal calculated by EDX analysis (10.9%) was almost equal to the theoretically computed value during catalyst synthesis. This could indicate the successful loading of active metal on support surface. However, boron element was not detected in the EDX analysis. Therefore, other advanced characterization techniques (including ATR-FTIR and XPS measurements) were further conducted in subsequent sections to confirm the presence of boron on catalysts.

3.2. X-ray diffraction measurements

The wide-angle XRD profiles of the mesoporous silica support and all the catalysts are shown in Fig. 2. The diffraction peaks at 2θ of 37.3°, 43.3°, 62.9° and 75.3° corresponding to (101), (012), (220) and (311) planes were detected, assigned to crystal planes of the cubic NiO phase (JCPDS card No. 47-1049) [27]. A broad peak centred at 2θ of 22.6° was observed in all the catalysts that can be ascribed to the amorphous nature of the silica framework (JCPDS card No. 29-0085) [28]. However, a peak at $2\theta = 27.8°$ that generally correspond to the facet (102) of B$_2$O$_3$ could not observed for boron promoted catalysts. This could be probably due to the high dispersion of B$_2$O$_3$ particles on SBA-15 support that might result in B$_2$O$_3$ crystallites with a smaller size which is beyond the XRD detection limit [29,30].

The mean crystallite size of nickel oxide in all the samples was calculated using line broadening of the most intense peak at (012) diffraction of NiO phase (see Eq. (1)). The crystallite size of NiO was estimated 14.5 nm in Ni/SBA-15 catalyst, which decreased to 11.7 nm and

Table 2
Physical properties of the SBA-15 support, NS and x%B-NS catalysts.

Physical properties	Average BET surface area (m^2 g^{-1})	[a]Average pore size (nm)	Total pore volume (cm^3 g^{-1})	[b]Average NiO crystallite size (nm)
SBA-15	669.8	7.1	1.2	–
NS	538.7	6.6	0.9	14.5
1%B-NS	411.4	6.7	0.7	11.7
2%B-NS	323.6	6.8	0.5	11.9
3%B-NS	215.6	6.6	0.3	14.2
5%B-NS	4.1	4.1	0.3	14.6

[a] Barrett-Joyner-Hallender (BJH) desorption method was used for estimation at P/P$_0$ = 0.99.
[b] Value was obtained from the most intensive NiO peak at $2\theta = 43.3°$ ((012) NiO plane) using Scherrer equation (1).
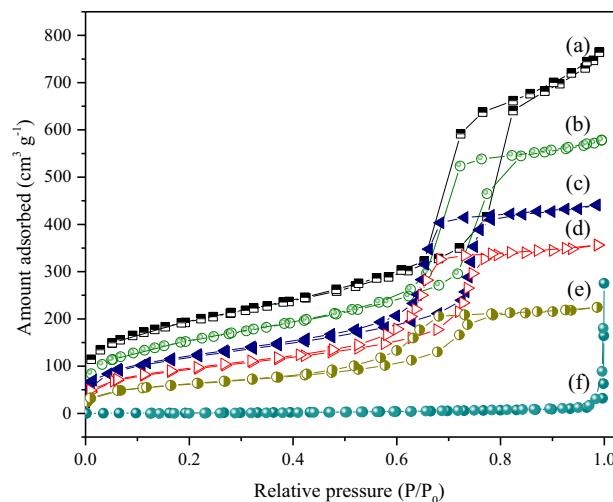
Fig. 1. N_2 adsorption-desorption isotherms of (a) SBA-15 support, (b) NS, (c) 1%B-NS, (d) 2%B-NS, (e) 3%B-NS and (f) 5%B-NS catalysts.
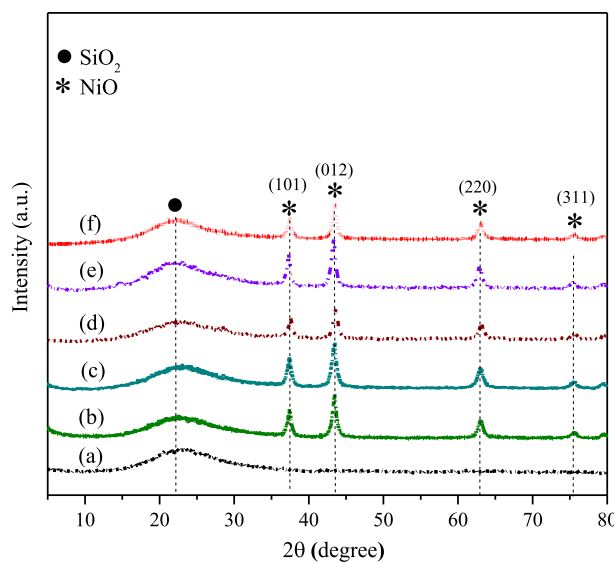

Fig. 2. XRD patterns of (a) SBA-15 support, (b) NS, (c) 1%B-NS, (d) 2%B-NS, (e) 3%B-NS and (f) 5%B-NS catalysts.

11.9 nm with the addition of 1% and 2% boron, respectively. The decrease in NiO crystal size with B-promoter addition could be possibly due to the dilution effect of a B_2O_3 promoter. This statement can be supported by the first principle density-functional theory calculations by Saeys et al. that demonstrated that boron could occupy the octahedral Ni (111) sites, which may isolate or dilute NiO particles and hence inhibiting their agglomeration [12]. However, a further increase in boron concentration increased crystallite size of NiO from 11.9 nm to 14.2 nm by increasing the boron loading from 2% to 3%. This can be explained with a fact that at excessive B loading, B_2O_3 particles could also reside on the SBA-15 support surface. Therefore, the diffusion competition between B_2O_3 and NiO particles on SBA-15 resulted in metal agglomeration. This phenomenon resulted in the substantial decrease in the surface area in the catalysts with higher concentration of boron, as confirmed by BET results discussed before.

3.3. H_2 temperature-programmed reduction analysis

Fig. 3 shows results of H_2-temperature-programmed reduction analysis of all the catalysts. At a glance, it can be observed from the results, a broad peak ranging from 600 to 890 K was detected which was deconvoluted to three peaks (P_1, P_2, and P_3). These three deconvoluted reduction peaks can be assigned to the presence of distinct kinds of NiO particles in catalysts. The first broad peak (P_1) appeared at 660—717 K could be ascribed to the reduction of large NiO particles located on the outer surface of the silica support with weak metal-support interaction. The second peak (P_2) centered at 690—760 K was assigned to NiO particles with moderate interaction with support [31] and the third peak (P_3) observed at 770—785 K can be ascribed to the reduction of highly dispersed NiO particles, which could be strongly interacted with SBA-15 support [32]. However, the B_2O_3 phase was found unreduced during H_2-TPR due to its high stability [32].

Furthermore, it is worth to mention that the first peak P_1 at 660 K in NS catalyst was slightly shifted to higher reduction temperature with the addition of boron, suggesting that the interaction between NiO and SBA-15 support was strengthened by incorporation of boron to the
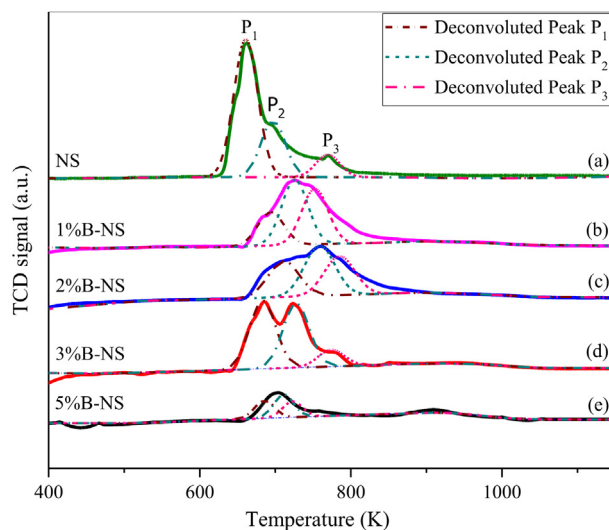
Fig. 3. H_2 temperature-programmed reduction of (a) SBA-15 support, (b) NS, (c) 1%B-NS, (d) 2%B-NS, (e) 3%B-NS and (f) 5%B-NS catalysts.

Ni/SBA-15 [33,34] and may also account for the smaller crystallite size of NiO particles observed in the XRD results. Additionally, the influence of boron loading on H_2-uptake from H_2-TPR measurement is displayed in Fig. S2 (supplementary data). The results showed that the amounts of H_2-consumption increased with the addition of boron, suggesting higher reduction for NiO particles. It can be assigned to high electron density on catalysts surface by boron promoter and thus increasing the reduction of NiO phase. However, a substantial drop in H_2-uptake was found with increasing boron loading from 2% to 5%, suggesting that the excess boron loading possibly covered the surface of NiO species and made it inaccessible from reacting hydrogen.

3.4. ATR-Fourier transform infrared spectroscopy analysis

ATR-FTIR spectroscopy was employed to examine the surface functionality of SBA-15 support after addition of NiO particles and B-promoter. The results are shown in Fig. 4. As one can observe from the results, a typical asymmetric (440 cm^{-1}) and symmetric (810 cm^{-1}) stretching vibration of Si-O bond and asymmetric stretching of Si-O-Si at 1050 cm^{-1} can be clearly detected in SBA-15 support and all the catalysts. These stretching vibrations signified the formation of siloxane network [35]. Additionally, a low-intensity peak located at 965 cm^{-1} corresponds to the typical vibration of silanol group (Si-OH), further confirming the mesoporosity of SBA-15 support [36]. These ATR-FTIR results are well in-line with BET studies. Furthermore, a band was detected at 670 cm^{-1} which can be assigned to B-O-Si bending vibration [31]. The strong adsorption band at 1378 cm^{-1} with the highest intensity for x%B-NS (x; 3% and 5%) catalysts was originated from the trigonal BO_3 units due to the excess of boron [37]. However, the peak appeared at 965 cm^{-1} corresponds to silanol band was not detected in boron promoted catalysts, indicating the basic sites of Si-OH were consumed by boric acid in these catalysts. Besides, an adsorption band originated at 920 cm^{-1} represents the stretching vibration of B-O that originated from tetrahedrally coordinated BO_4 species [38].
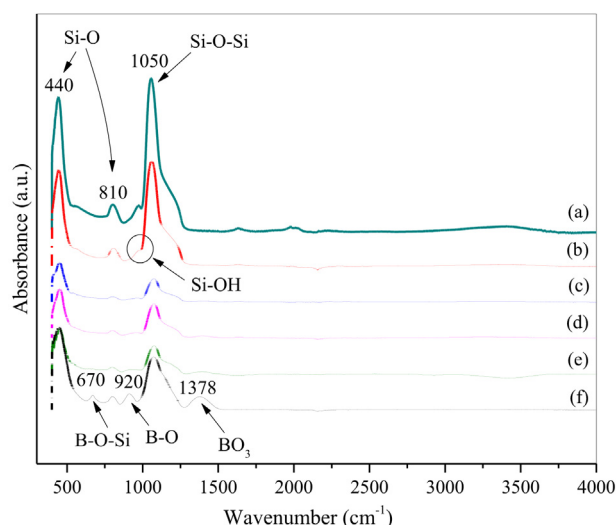
Fig. 4. ATR-FTIR spectra of (a) SBA-15 support, (b) NS, (c) 1%B-NS, (d) 2%B-NS, (e) 3%B-NS and (f) 5%B-NS catalysts.

One of the recent studies have suggested that B-OH possesses better protonation ability compared to silanol groups, besides 1 mol of H_3BO_3 generates 1 mol of Si-O-B(OH)-O-Si and 2 mol of Si-OH groups [39]. Furthermore, these functionalities (i.e., B-OH and silanol species) contributed to increase the number of active oxygen sites. Ni et al. postulated that the B-OH species generated from the rehydration of trigonal BO_3 units (at 1378 cm^{-1}) have a great potential to remove the deposited carbon during the DRM reaction [17]. The CO_2 adsorbed with B-OH species converts it to hydrocarbonates (HCO_3^-)/carbonates (CO_3^{2-}) which further reacts with the H atoms produced during the methane cracking to form formate (HCO_2^-) intermediates and subsequently decompose to CO and OH groups. The existence of these B-OH species in the mesoporous silica framework would improve the oxygen mobility and prevent the carbon formation on the surface of boron promoted catalysts.

3.5. X-ray photoelectron spectroscopy analysis

X-ray photoelectron spectroscopy (XPS) measurement of the selected 2%B-promoted catalyst is presented in Figs. S3 and S4 (supplementary data). As seen in Fig. S3, the full survey scan XPS spectrum features the peaks of Ni 2p (i.e., Ni 2p$_{1/2}$ and Ni 2p$_{3/2}$), C 1s, Si 2s, Si 2p$_{3/2}$ and O 1s [40]. In addition, a peak at binding energy of 188.1 eV corresponding to B 1s was detected for 2%B-NS (see the inset of Fig. S3 in supplementary data), confirming the presence of boron oxide in the catalyst [41]. As seen in the expanded Ni 2p$_{3/2}$ XPS spectrum (Fig. S4 of supplementary data), the detected binding energies of Ni 2p$_{3/2}$ core line and satellite peak at the corresponding 856.6 and 862.4 eV could indicate the presence of NiO particles on SBA-15 support [42] in agreement with XRD results (see Fig. 2).

3.6. Catalytic performance for dry reforming of methane

Fig. 5 shows the results of DRM catalytic activity of NS and x%B-NS catalysts. The results demonstrated that the reactant conversion was considerably increased with the addition of boron to the SBA-15 supported nickel catalyst. Evidently, NS catalyst showed CH_4 and CO_2 conversion of 67.9% and 77.4%, respectively. Moreover, the catalyst with 1% and 2% boron showed highest conversion for CH_4 and CO_2 which were about 90% and 92%, respectively whereas the further increase in boron concentration could not achieve the competitive results. The higher activity of these catalyst can be attributed to the synergistic effect of high BET surface area and lower crystallite size that greatly improved the accessibility of active sites. On the other hand, in the catalysts with 3% and 5% boron, extensively high B_2O_3 content inevitably blocked or covered the accessible active nickel surface by increasing the agglomeration, hence substantially reduced CH_4 and CO_2 conversions. In fact, the severe loss of catalytic activity for 5%B-NS catalyst (about 2.6 and 1.9 times of CH_4 and CO_2 conversions, respectively) compared to the 1%B promoted counterparts was observed. It can be attributed to poor textural properties of 5%B-promoted catalyst (see Table 2), which strongly affected the dispersion or accessibility of active metal surface sites. Interestingly, a similar trend in H_2-uptake and conversion of catalysts can be seen in supplementary data (see Fig. S2), thus it can be deduced that degree of H_2 reduction is a crucial factor for improving the catalytic performance. Additionally, the conversion of the reactants was stable during the span of 10 h, except for 1% of boron which showed a slight decline of about 5.6% and 3.1% for corresponding CH_4 and CO_2 conversions, respectively, compared to the initial activity. This behaviour might be due to the formation of partially dehydrogenated carbon (CH_x) species on the catalyst surface, which blocked the active metal sites and reduced its activity with time-on-stream. However, to get a better insight into the type and amount of carbon, al the spent catalysts were further studied by using XRD, Raman, TPO and HR-TEM measurements.

As shown in Fig. 5(c), H_2/CO ratio was always less than 1 due to unavoidable RWGS reaction. Irrespective of the catalyst, CO yield was greater than the H_2 yield as displayed in Fig. S5 (see supplementary data). Interestingly, the difference between H_2 and CO yield was comparatively smaller for x%B-NS catalyst (x $\leq$ 2%), indicating that better dispersion and high accessibility to active sites could efficiently control the occurrence of RWGS in DRM reaction. Similar trends were observed for the H_2 and CO selectivity results as seen in Fig. S6 (supplementary data).

In addition, many studies have been previously extolled the benefits of boron on different support materials and reactions [13,31,43]. For example, one of the studies showed the conversion of CH_4 and CO_2 was 55% and 65%, respectively during DRM reaction at 973 K for Ni/Al_2O_3 catalyst. However, the addition of boron lead to decrease in conversion of reactants [15]. In one of the recent studies, Ni et al. successfully applied the borated alumina supported nickel catalyst for DRM reaction and showed that 5% boron promoted catalyst exhibited the highest activity and stability than 1% and 10% boron promoted catalyst for 65 h longevity test at 973 K [17]. However, in this work, a small amount of boron (x $\leq$ 2%) was enough to enhance the catalytic activity, which is a good factor for the economic viability of catalyst and its industrial implementation.

3.7. Characterization of spent catalysts

#### 3.7.1. X-ray diffraction measurements for spent catalysts
Fig. 6 shows the XRD profiles of x%B-NS and unpromoted spent NS catalysts. The catalysts were activated in-situ at 1023 K with 50%H_2/N_2 at ramping of 5 K min^{-1}. On can see in the results, three sharp peaks were consistently observed in all spent catalysts, corresponding to the (110), (200) and (220) facets at 2θ of 44.6°, 51.9° and 76.4°, respectively of metallic nickel. The results are consistent with the standard data, JCPDS card No. 04-0850 [44,45]. In addition, the typical NiO phases (JCPDS card No. 47-1049) were not noticed in all the catalysts, suggesting that the catalysts were not re-oxidized during DRM reaction. A small peak at 2θ of 26.2° corresponding to (002) plane was detected for 1%B-Ni/SBA-15 catalyst which represents the formation of crystalline graphitic carbon or multiwalled carbon nanotubes (MWNTs) [46,47]. Interestingly, this peak was not detected in the catalysts with higher boron concentration. This might be due to the presence of oxygen sites (i.e. B-OH and Si-OH) for high boron loading catalysts as detected in FT-IR spectra results. These sites may play a critical role to inhibit the carbon formation and provide greater stability in DRM reaction.
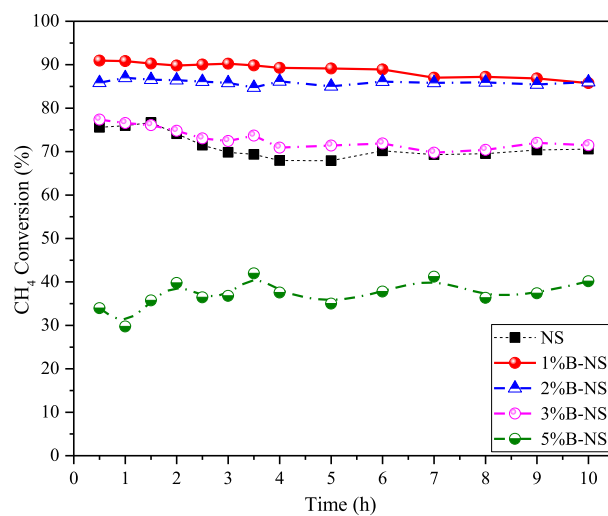
(a)
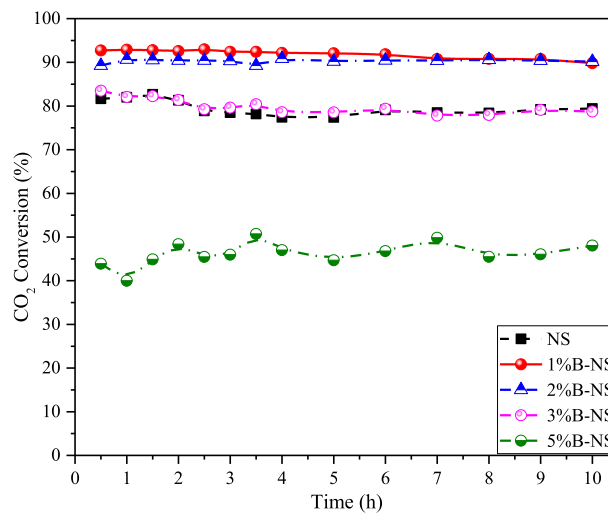
(b)
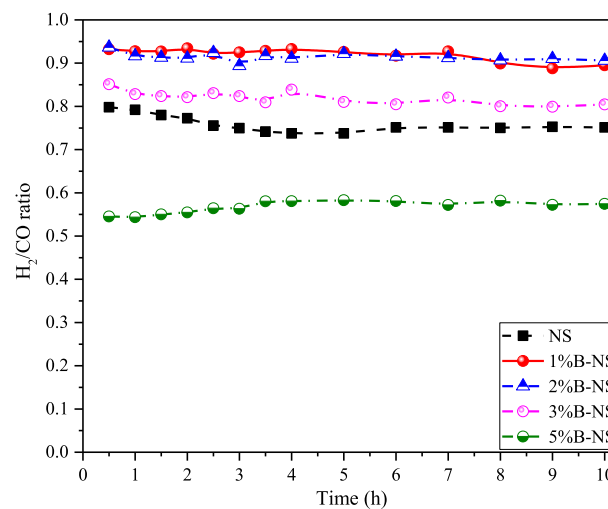
(c)

Fig. 5. Effect of boron loading on (a) CH_4 conversion, (b) CO_2 conversion, and (c) H_2/CO ratio at 1023 K with stoichiometric feed ratio: $Q_{CH_4} : Q_{CO_2} = 1 : 1$ and 10 h time-on-stream for DRM reaction.
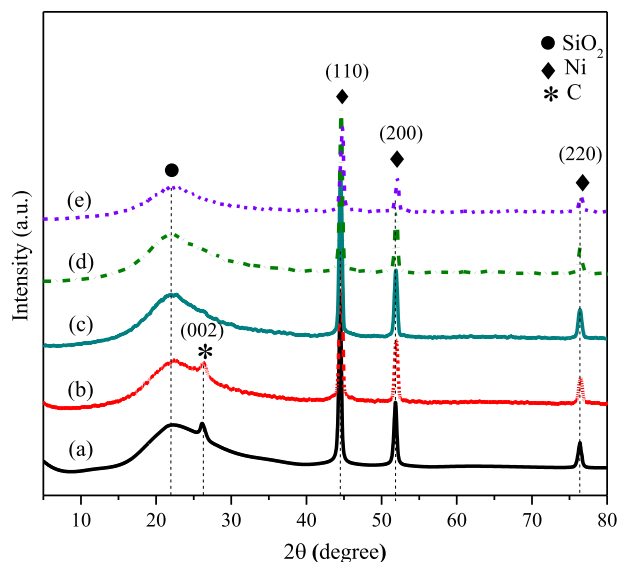
Fig. 6. XRD spectra of spent (a) NS, (b) 1%B-NS, (c) 2%B-NS, (d) 3%B-NS and (e) 5%B-NS catalysts.

3.7.2. Raman spectroscopy measurements

Fig. 7 shows results of Raman spectroscopy of boron promoted and unpromoted spent Ni/SBA-15 catalysts. The results showed that Raman spectra for pure SBA-15 support exhibited a Raman shift at about 1064.9 cm^{-1}, corresponding to the stretching vibration of Si-O, supported with the ATR-FTIR results [48]. However, this peak was not detected in the catalyst with for 5% boron. Moreover, Raman spectra displayed two main peaks centered at 1335 cm^{-1} and 1570 cm^{-1}, corresponding to D and G band for unpromoted catalyst and 1% boron promoted spent catalyst. The D band can be attributed to disordered or amorphous induced band, arising from the breathing modes of the sp^2 hybridization atoms in the graphite layers, whereas G band represents E_{2g} vibration mode of stretching in-plane vibration for carbon-carbon bonds in the graphitic layers [49,50]. However, these bands were not detected in the catalysts with higher concentration of boron ($\geq$1%), indicating that the higher boron content remarkably inhibited the carbon deposition.

The relative intensity of D and G bands was further used to express the degree of graphitization in the spent catalyst after DRM reaction, the results are depicted in Table 3, which demonstrated that I_D/I_G ratio for 1% boron promoted catalysts (0.59) was lower than the unpromoted catalyst (0.70). However, high value of I_G compared to I_D for 1%B-NS catalyst, indicating the presence of higher amount of graphitic carbon than amorphous carbonaceous species.

3.7.3. Temperature-programmed oxidation (TPO) analysis

Fig. 8 illustrates the derivative weight for NS catalyst and x%B-NS (x $\leq$ 2%) showed the presence of the two distinct peaks (P_1 and P_2) of the CO_2 desorption at about 562 K (P_1) and 865 K (P_2), corresponding to amorphous and graphitic carbonaceous species, respectively. One could notice the presence of small intensity peaks at 595 K for amorphous carbons (P_1) for 1% boron promoted catalyst. However, the intensity of peak P_2 at 915 K is comparatively similar to unpromoted catalyst. It clearly indicates that amorphous carbon was removed by the
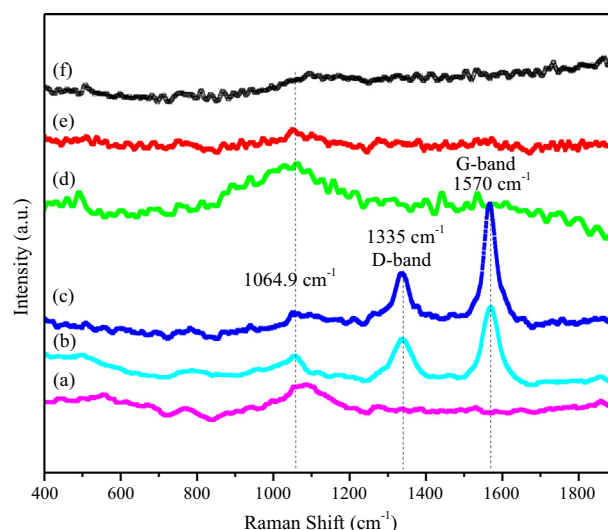

Fig. 7. Raman spectra of (a) SBA-15 support, (b) NS, (c) 1%B-NS, (d) 2%B-NS, (e) 3%B-NS and (f) 5%B-NS spent catalysts.

Table 3
Summary of average crystallite size, I_D/I_G and carbon deposition on the spent NS and x%B-NS catalysts after DRM reaction at 1023 K with stoichiometric feed ratio: $Q_{CH_4} : Q_{CO_2} = 1 : 1$ and 10 h time-on-stream.

Spent Catalysts	Average Crystallite size of Ni (nm)	I_D/I_G ratio	Weight loss (%)
NS	25.2	0.70	14.0
1%B-NS	25.8	0.59	6.5
2%B-NS	27.4	−	1.3
3%B-NS	26.9	−	−
5%B-NS	20.5	−	−
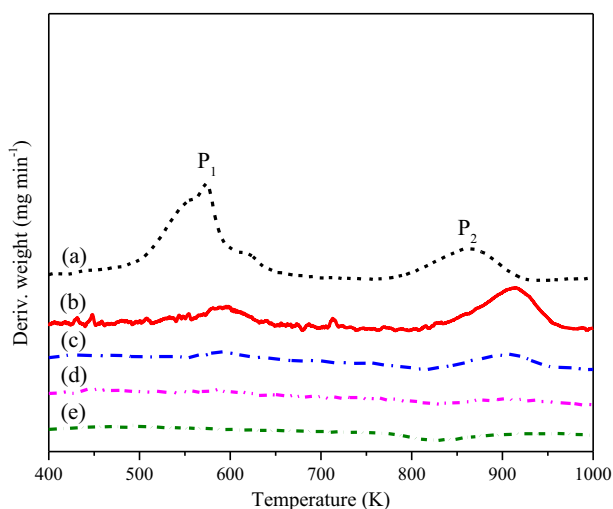
Fig. 8. TPO profiles of spent (a) NS, (b) 1%B-NS, (c) 2%B-NS, (d) 3%B-NS and (e) 5%B-NS catalysts.
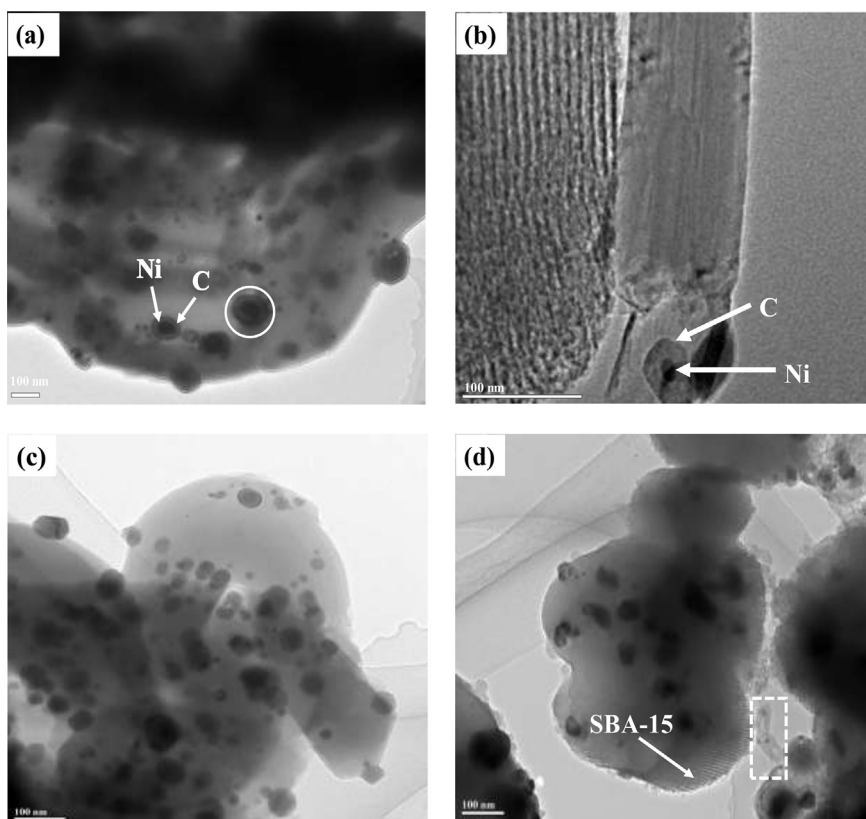
Fig. 9. HRTEM images of spent (a) NS, (b) 1%B-NS, (c) 2%B-NS and (d) 5%B-NS catalysts.

boron oxide species, while the graphitic carbon was unaltered by a small amount of boron (1%) in the catalyst. However, the peaks were completely disappeared for the high boron content (x%B-NS (x $\geq$ 2%)) catalyst, which further validating the information from Raman and XRD results. In fact, the weight loss percentage of about 14.0%, 6.5%, 1.3% was observed for the corresponding unpromoted catalyst, 1% and 2% boron catalyst, respectively (see Fig. S7 of supplementary data), whilst the weight loss profile for the high amount of boron (3% and 5%) content displayed no carbon deposition catalyst, proved the crucial role of boron to remove carbon.

3.7.4. HR-TEM measurements for spent catalysts

The spent catalysts were analyzed by HR-TEM analysis to investigate the type of deposited carbon, as shown in Fig. 9. The magnified images of NS and 1%B-NS catalysts are reasonable to infer that most of the nickel particles were encapsulated inside graphitic layers or shell-like carbons (also known as onion-like carbons). On the contrary, a very small multi-walled nanotube or herringbone hollow type carbonaceous species were observed for 5%B-NS catalyst, suggesting that few metallic nickel particles with weak interaction with the support might be carried away from the support by coke (as shown in Fig. 9(d) with dashed rectangle) [32]. In addition, negligible carbon was found for the 2%B-promoted catalyst, possibly due to higher nickel-support interaction observed in H_2-TPR (as shown in Fig. 3(c)) and hinder the removal and encapsulation of nickel by carbon in the reaction [51]. Therefore, it can be concluded from the results that encapsulating carbon surrounding the nickel particles could be considered as route cause for deactivation of the catalyst, which was negligibly formed during DRM reaction for higher boron promoted catalyst.

4. Conclusions

The ordered mesoporous SBA-15 support, NS and x%B-NS (1% $\leq$ x $\leq$ 5%) catalysts were successfully synthesized by using SIWI technique. The catalysts were tested for the DRM reaction at 1023 K with P_{CH_4} = 20 kPa and P_{CO_2} = 20 kPa for 10 h time-on-stream. The findings demonstrated that 1% and 2% boron-promoted catalysts not only enhanced the conversion of CH_4 and CO_2 to about 90% and 92%, respectively but also controlled the particle size of nickel oxide particles. On the other hand, high boron contents (3% and 5%) covered the pores of SBA-15 support and hence significantly affected the framework of SBA-15 support, resulting in low catalytic activity. The spent catalyst results showed that the unpromoted catalyst and 1%B-promoted catalyst exhibited both amorphous and graphitic carbons. Furthermore, the carbon formation was effectively controlled by increasing the boron loading in x%B-NS (x $\leq$ 1%) catalysts. The results show that B-OH species generated from the rehydration of BO_3 units could facilitate the gasification of deposited carbon.

Acknowledgements

Appendix A. Supplementary data

Supplementary data to this article can be found online at https://doi.org/10.1016/j.joei.2019.04.011.

References

[1] D. Li, Y. Nakagawa, K. Tomishige, Methane reforming to synthesis gas over Ni catalysts modified with noble metals, Appl. Catal., A 408 (2011) 1—24.
[2] T.J. Siang, S. Singh, O. Omoregbe, L.G. Bach, N.H.H. Phuc, D.-V.N. Vo, Hydrogen production from CH_4 dry reforming over bimetallic Ni-Co/Al_2O_3 catalyst, J. Energy Inst. 91 (2018) 683—694.
[3] X. Li, D. Li, H. Tian, L. Zeng, Z.J. Zhao, J. Gong, Dry reforming of methane over Ni/La2O3 nanorod catalysts with stabilized Ni nanoparticles, Appl. Catal., B 202 (2017) 683—694.
[4] L. Yao, M.E. Galvez, C. Hu, P. Da Costa, Synthesis gas production via dry reforming of methane over manganese promoted nickel/cerium-zirconium oxide catalyst, Ind. Eng. Chem. Res. (2018), https://doi.org/10.1021/acs.iecr.8b04183.
[5] S. Li, J. Gong, Strategies for improving the performance and stability of Ni-based catalysts for reforming reactions, Chem. Soc. Rev. 43 (2014) 7245—7256.
[6] D. Li, L. Zeng, X. Li, X. Wang, H. Ma, S. Assabumrungrat, J. Gong, Ceria-promoted Ni/SBA-15 catalysts for ethanol steam reforming with enhanced activity and resistance to deactivation, Appl. Catal., B 176—177 (2015) 532—541.
[7] Y. Yang, C. Ochoa-Hernández, P. Pizarro, A. Víctor, J.M. Coronado, D.P. Serrano, Ce-promoted Ni/SBA-15 catalysts for anisole hydrotreating under mild conditions, Appl. Catal., B 197 (2016) 206—213.
[8] J.C.S. Araujo, D. Zanchet, R. Rinaldi, U. Schuchardt, C.E. Hori, J.L.G. Fierro, J.M.C. Bueno, The effects of La_2O_3 on the structural properties of La_2O_3-Al_2O_3 prepared by the sol—gel method and on the catalytic performance of Pt/La_2O_3-Al_2O_3 towards steam reforming and partial oxidation of methane, Appl. Catal., B 84 (2008) 552—562.
[9] N.A. Pechimuthu, K.K. Pant, S.C. Dhingra, Deactivation studies over Ni-K/CeO_2-Al_2O_3 catalyst for dry reforming of methane, Ind. Eng. Chem. Res. 46 (2017) 1731—1736.
[10] H. Zhang, M. Li, P. Xiao, D. Liu, C.J. Zou, Structure and catalytic performance of Mg-SBA-15-Supported nickel catalysts for CO_2 reforming of methane to syngas, Chem. Eng. Technol. 6 (2013) 1701—1707.
[11] J.D. Bellido, J.E. De Souza, J.C. M'Peko, E.M. Assaf, Effect of adding CaO to ZrO_2 support on nickel catalyst activity in dry reforming of methane, Appl. Catal., A 358 (2009) 215—223.
[12] M. Saeys, K.F. Tan, J. Chang, A. Borgna, Improving the stability of cobalt Fischer-Tropsch catalysts by boron promotion, Ind. Eng. Chem. Res. 49 (2010) 11098—11100.
[13] J. Xu, L. Chen, K.F. Tan, A. Borgna, M. Saeys, Effect of boron on the stability of Ni catalysts during steam methane reforming, J. Catal. 261 (2009) 158—165.
[14] K.F. Tan, J. Chang, A. Borgna, M. Saeys, Effect of boron promotion on the stability of cobalt Fischer—Tropsch catalysts, J. Catal. 280 (2011) 50—59.
[15] A. Fouskas, M. Kollia, A. Kambolis, C. Papadopoulou, H. Matralis, Boron-modified Ni/Al_2O_3 catalysts for reduced carbon deposition during dry reforming of methane, Appl. Catal., A 474 (2014) 125—134.
[16] Y. Cao, M. Lu, J. Fang, L. Shi, D. Zhang, Hexagonal boron nitride supported mesoSiO2-confined Ni catalysts for dry reforming of methane, ChemCommun (Camb) 53 (2017) 7549—7552.
[17] J. Ni, L. Chen, J. Lin, S. Kawi, Carbon deposition on borated alumina supported nano-sized Ni catalysts for dry reforming of CH_4, Nanomater. Energy 1 (2012) 674—686.
[18] Z. Taherian, M. Yousefpour, M. Tajally, B. Khoshandam, A comparative study of ZrO_2 , Y_2O_3 and Sm_2O_3 promoted Ni/SBA-15 catalysts for evaluation of CO_2/methane reforming performance, Int. J. Hydrogen Energy 42 (2017) 16408—16420.
[19] Z. Taherian, M. Yousefpour, M. Tajally, B. Khoshandam, Promotional effect of samarium on the activity and stability of Ni-SBA-15 catalysts in dry reforming of methane, Microporous Mesoporous Mater. 251 (2017) 9—18.
[20] J. Zhu, X. Peng, L. Yao, D. Tong, C. Hu, CO_2 reforming of methane over Mg-promoted Ni/SiO_2 catalysts: the influence of Mg precursors and impregnation sequences, Catal. Sci. Technol. 2 (2012) 529—537.
[21] A. Albarazi, M.E. Gálvez, P. Da Costa, Synthesis strategies of ceria-zirconia doped Ni/SBA-15 catalysts for methane dry reforming, Catal. Commun. 59 (2015) 108—112.

[22] U. Oemar, Y. Kathiraser, L. Mo, X.K. Ho, S. Kawi, CO_2 reforming of methane over highly active La-promoted Ni supported on SBA-15 catalysts: mechanism and kinetic modelling, Catal. Sci. Technol. 2016 (6) (2016) 1173—1186.

[23] A.L. Patterson, The Scherrer formula for X-ray particle size determination, Phys. Rev. 56 (1939) 978—982.

[24] N. Wang, K. Shen, L. Huang, X. Yu, W. Qian, W. Chu, Facile route for synthesizing ordered mesoporous Ni-Ce-Al oxide materials and their catalytic performance for methane dry reforming to hydrogen and syngas, ACS Catal. 3 (2013) 1638—1651.

[25] S. Singh, R. Kumar, H.D. Setiabudi, S. Nanda, D.-V.N. Vo, Advanced synthesis strategies of mesoporous SBA-15 supported catalysts for catalytic reforming applications: a state-of-the-art review, Appl. Catal., A 559 (2018) 57—74.

[26] S. Zhu, X. Gao, Y. Zhu, Y. Zhu, H. Zheng, Y. Li, Promoting effect of boron oxide on Cu/SiO_2 catalyst for glycerol hydrogenolysis to 1, 2-propanediol, J. Catal. 303 (2013) 70—79.

[27] JCPDS Powder Diffraction File, International Center for Diffraction Data, Swarthmore, PA, 2000.

[28] A.J. Vizcaíno, A. Carrero, J.A. Calles, Comparison of ethanol steam reforming using Co and Ni catalysts supported on SBA-15 modified by Ca and Mg, Fuel Process. Technol. 146 (2016) 99—109.

[29] D. Kang, J.W. Lee, Enhanced methane decomposition over nickel-carbon-B_2O_3 core-shell catalysts derived from carbon dioxide, Appl. Catal., B 186 (2016) 41—55.

[30] X. Chen, S. Wang, J. Zhuang, M. Qiao, K. Fan, H. He, Mesoporous silica-supported NiB amorphous alloy catalysts for selective hydrogenation of 2-ethylanthraquinone, J. Catal. 227 (2004) 419—427.

[31] H. Chen, J. Tan, J. Cui, X. Yang, H. Zheng, Y. Zhu, Y. Li, Promoting effect of boron oxide on Ag/SiO_2 catalyst for the hydrogenation of dimethyl oxalate to methyl glycolate, Mol. Catal. 433 (2017) 346—353.

[32] J.A. Calles, A. Carrero, A.J. Vizcaíno, L. García-Moreno, Hydrogen production by glycerol steam reforming over SBA-15-supported nickel catalysts: effect of alkaline earth promoters on activity and stability, Catal. Today 227 (2014) 198—206.

[33] T.J. Siang, T.L. Pham, N. Van Cuong, P.T. Phuong, N.H.H. Phuc, Q.D. Truong, D.-V.N. Vo, Combined steam and CO_2 reforming of methane for syngas production over carbon-resistant boron-promoted Ni/SBA-15 catalysts, Microporous Mesoporous Mater. 262 (2018) 122—132.

[34] J. Zheng, Z. Xia, J. Li, W. Lai, X. Yi, B. Chen, W. Fang, H. Wan, Promoting effect of boron with high loading on Ni-based catalyst for hydrogenation of thiophene-containing ethylbenzene, Catal. Commun. 21 (2012) 18—21.

[35] X. Huang, W. Li, M. Wang, X. Tan, Q. Wang, C. Wang, M. Zhang, J. Yuan, A facile template route to periodic mesoporous organosilicas nanospheres with tubular structure by using compressed CO_2, Sci. Rep. 7 (2017) 45055.

[36] S. Aslam, F. Subhan, Z. Yan, Z. Liu, R. Ullah, U.J. Etim, W. Xing, Unusual nickel dispersion in confined spaces of mesoporous silica by one-pot strategy for deep desulfurization of sulfur compounds and FCC gasoline, Chem. Eng. J. 2017 (321) (2017) 48—57.

[37] G.P. Heitmann, G. Dahlhoff, J.P.M. Niederer, W.F. Hölderich, Active sites of a [B]-ZSM-5 zeolite catalyst for the Beckmann rearrangement of cyclohexanone oxime to caprolactam, J. Catal. 194 (2000) 122—129.

[38] S.C. Neumair, R. Kaindl, R.D. Hoffmann, H. Huppertz, The new high-pressure borate hydrate $Cu_3B_6O_{12} \cdot H_2O$, Solid State Sci. 14 (2012) 229—235.

[39] W. Zhang, D. Yu, X. Ji, H. Huang, Efficient dehydration of bio-based 2,3-butanediol to butanone over boric acid modified HZSM-5 zeolites, Green Chem. 14 (2012) 3441—3450.

[40] T.J. Siang, L.G. Bach, S. Singh, Q.D. Truong, N.H.H. Phuc, F. Alenazey, D.V.N. Vo, Methane bi-reforming over boron-doped Ni/SBA-15 catalyst: longevity evaluation, Int. J. Hydrogen Energy (2018), https://doi.org/10.1016/j.ijhydene.2018.06.123.

[41] H. Li, H. Li, J.F. Deng, Glucose hydrogenation over $Ni-B/SiO_2$ amorphous alloy catalyst and the promoting effect of metal dopants, Catal. Today 74 (2002) 53—63.

[42] A. Rodriguez-Gomez, R. Pereñiguez, A. Caballero, Understanding the differences in catalytic performance for hydrogen production of Ni and Co supported on mesoporous SBA-15, Catal. Today 307 (2018) 224—230.

[43] E. Romeo, M. Saeys, A. Monzón, A. Borgna, Carbon nanotube formation during propane decomposition on boron-modified Co/Al_2O_3 catalysts: a kinetic study, Int. J. Hydrogen Energy 39 (2014) 18016—18026.

[44] W. Li, Z. Zhao, X. Guo, G. Wang, Employing a nickel-containing supramolecular framework as Ni precursor for synthesizing robust supported Ni catalysts for dry reforming of methane, ChemCatChem 8 (2016) 2939—2952.

[45] J. Zhang, F. Li, Coke-resistant Ni@ SiO_2 catalyst for dry reforming of methane, Appl. Catal., B 176—177 (2015) 513—521.

[46] Y.J. Asencios, E.M. Assaf, Combination of dry reforming and partial oxidation of methane on $NiO-MgO-ZrO_2$ catalyst: effect of nickel content, Fuel Process. Technol. 106 (2013) 247—252.

[47] S. Yasyerli, S. Filizgok, H. Arbag, N. Yasyerli, G. Dogu, Ru incorporated Ni-MCM-41 mesoporous catalysts for dry reforming of methane: effects of Mg addition, feed composition and temperature, Int. J. Hydrogen Energy 36 (2011) 4863—4874.

[48] G. Hu, W. Li, J. Xu, G. He, Y. Ge, Y. Pan, J. Wang, B. Yao, Substantially reduced crystallization temperature of SBA-15 mesoporous silica in $NaNO_3$ molten salt, Mater. Lett. 170 (2016) 179—182.

[49] S. Zhang, S. Muratsugu, N. Ishiguro, M. Tada, Ceria-doped Ni/SBA-16 catalysts for dry reforming of methane, ACS Catal. 2013 (3) (2013) 1855—1864.

[50] K.Y. Koo, S.H. Lee, U.H. Jung, H.S. Roh, W.L. Yoon, Syngas production via combined steam and carbon dioxide reforming of methane over $Ni-Ce/MgAl_2O_4$ catalysts with enhanced coke resistance, Fuel Process. Technol. 119 (2014) 151—157.

[51] M. Tao, Z. Xin, X. Meng, Z. Bian, Y. Lv, Highly dispersed nickel within mesochannels of SBA-15 for CO methanation with enhanced activity and excellent thermostability, Fuel 188 (2017) 267—276.